Kanehisa, *Biochem. Biophys. Res. Commun.* **138**, 568 (1986). Comparisons of the ASL and δ-crystallin sequences with those for tetrameric, 50-kD subunit size bacterial aspartases and fumarases show regions of similarity (G. Wistow and J. Piatigorsky, unpublished results).

14. L. A. Williams, L. Ding, J. Horwitz, J. Piatigorsky, *Exp. Eye Res.* **40**, 741 (1985).
15. τ-Crystallin was purified from adult turtle lens by isoelectric focusing, followed by chromatography on a TSK 3000 SW gel permeation column, then on a Synchro Pak AX 300 anion-exchange column [L. A. Williams and J. Horwitz (*14*)]. Protein sequencing was performed by W. S. Lane and D. Andrews, Harvard University Microchemistry Facility, Harvard University, Cambridge, MA 02138. V8-proteolytic fragments of turtle τ-crystallin were separated by high-performance liquid chromatography (HPLC). Some peptides of major yield were then sequenced by an automated AP 470 sequencer. All peptides sequenced showed strong similarity to human α-enolase.
16. A. Giallongo, S. Feo, R. Moore, C. M. Croce, L. C. Showe, *Proc. Natl. Acad. Sci. U.S.A.* **83**, 6741 (1986); C. C. Q. Chin, J. M. Brewer, F. Wold, *J. Biol. Chem.* **256**, 1337 (1981).
17. O. Hockwin and C. Ohrloff, in *Molecular and Cellular Biology of the Eye Lens*, H. Bloemendal, Ed. (Wiley, New York, 1981), pp. 367–413.
18. L. M. Matrisian, G. Rautmann, D. I. Magun, R. Breathnach, *Nucleic Acids Res.* **13**, 711 (1985).
19. J. J. Picard *et al.*, *Exp. Cell Res.* **167**, 157 (1986).
20. J. A. Cooper, N. A. Reiss, R. J. Schwartz, T. Hunter, *Nature (London)* **302**, 218 (1983).
21. I. MacDonald, J. Levy, T. Pawson, *Mol. Cell. Biol.* **5**, 2543 (1985).
22. K. R. Williams, S. Reddigari, G. L. Patel, *Proc. Natl. Acad. Sci. U.S.A.* **82**, 5260 (1985).
23. H. Iida and I. Yahara, *Nature (London)* **315**, 688 (1985).
24. A. Packard, *Biol Rev.* **47**, 241 (1972).
25. R. J. Siezen and D. C. Shaw, *Biochim. Biophys. Acta* **704**, 304 (1982).
26. H.-C. J. Lai, N. Li, M. J. Weiss, C. C. Reddy, C.-P. D. Tu, *J. Biol. Chem.* **259**, 5536 (1984).
27. W. B. Jakoby, *Adv. Enzymol.* **44**, 383 (1978).
28. Relative enolase activity was measured according to the method of E. W. Westhead [*Methods Enzymol.* **9**, 670 (1967)]. ASL activity was measured according to the method of S. Ratner [*ibid.* **17**, 304 (1970); also W. E. O'Brien, unpublished]. GST activity in lens homogenate of commercially available squid was measured according to the procedure of W. A. Habig, M. J. Pabst, and W. B. Jakoby [*J. Biol. Chem.* **249**, 7130 (1974)].

29. We thank L. Williams and J. Horwitz for the turtle τ-crystallin, and W. E. O'Brien, W. W. de Jong, R. F. Doolittle, W. B. Jakoby, and J. Nickerson for helpful discussions, and D. Chicchirichi for manuscript preparation.

22 January 1987; accepted 14 April 1987

Alpha-Decay–Induced Fracturing in Zircon: The Transition from the Crystalline to the Metamict State

BRYAN C. CHAKOUMAKOS, TAKASHI MURAKAMI,*
GREGORY R. LUMPKIN, RODNEY C. EWING

A natural single crystal of zircon, $ZrSiO_4$, from Sri Lanka exhibited zonation due to alpha-decay damage. The zones vary in thickness on a scale from one to hundreds of micrometers. The uranium and thorium concentrations vary from zone to zone such that the alpha-decay dose is between 0.2×10^{16} and 0.8×10^{16} alpha-events per milligram (0.15 to 0.60 displacement per atom). The transition from the crystalline to the aperiodic metamict state occurs over this dose range. Differential expansion of individual layers due to variations in their alpha-decay dose caused a systematic pattern of fractures that do not propagate across aperiodic layers. High-resolution transmission electron microscopy revealed a systematic change in the microstructure from a periodic atomic array to an aperiodic array with increasing alpha-decay dose. At doses greater than 0.8×10^{16} alpha-events per milligram there is no evidence for long-range order. This type of damage will accumulate in actinide-bearing, ceramic nuclear waste forms. The systematic pattern of fractures would occur in crystalline phases that are zoned with respect to actinide radionuclides.

ZIRCON, $ZrSiO_4$, OCCURS IN NATURE with total uranium and thorium concentrations that are usually in the range from 0 to 4000 ppm (*1*) but in rare cases up to 6% by weight $UO_2 + ThO_2$ (*2*). Alpha-decay doses over hundreds of millions of years can be as high as 10^{17} alpha-events per milligram, which is equivalent to 7 displacements per atom (dpa). Over the narrow dose range from 10^{15} to 10^{16} alpha-events per milligram (Fig. 1), crystalline zircon is converted to the metamict state, a structure that appears to be amorphous when analyzed by x-ray and electron diffraction. The transition causes pronounced changes in physical properties [for example, a decrease in density (17%) (*3*), a decrease in birefringence until the material is isotropic (*3*), a decrease in the elastic moduli (up to 69%) (*4*), and a decrease in Poisson's ratio (7%) (*4*)]. Plutonium-doped synthetic zircons show approximately the same density change (16%) at doses of 10^{16} alpha-events per milligram (*5*). With increasing alpha-decay dose, x-ray diffraction maxima decrease in intensity, become asymmetric, and shift to lower values of 2θ (because of a unit cell volume expansion of 5%, where θ is the angle between the diffracting plane and the x-ray beam) until the material becomes amorphous to x-ray diffraction (*3, 6*). Individual samples that spanned portions of the transition-dose zone have been studied by transmission electron microscopy, but to our knowledge no high-resolution electron microscopy study has spanned the full range of doses over which the transition occurs (*7, 8*).

The changes in the atomic structure and accompanying changes in physical properties caused by alpha-decay damage are of significance for several reasons. (i) Zircon is a major mineral used in dating igneous and metamorphic rocks by U-Th-Pb methods. Disturbed U-Th-Pb systematics have been ascribed to alpha-decay damage (*9*). (ii) The zircon structure type is an actinide-bearing phase in multiphase ceramic nuclear waste forms (*10*), and natural zircon has been used to evaluate elemental loss from waste form phases under repository conditions (*11*). The change in the atomic structure during the transition is fundamental to the evaluation of the long-term performance of crystalline, polyphase, ceramic nuclear waste forms (*12, 13*). In this report we present data on a zoned zircon from Sri Lanka (Ceylon) in which the variation in the UO_2 and ThO_2 contents from zone to zone is such that the range of dose varies from 0.2×10^{16} to 0.8×10^{16} alpha-events per milligram (equivalent to 0.15 to 0.60 dpa) and thus covers the most important range of dose over which the radiation-induced crystalline-to-metamict transition occurs (Fig. 1).

The single crystal was collected from the gem gravels of the Ratnapura district in Sri Lanka (*14*). The age of the zircons is 570 ± 20 million years (*3*). Although the provenance of these alluvial zircons is problematic, their large size, internal growth zoning, and lack of metamorphic deformation suggest that they are magmatic; their likely source rocks are granitoid plutons or pegmatites. The prismatic crystal (sample 4601 University of New Mexico Research Collection) was sectioned lengthwise to expose an unbanded core capped by coarse (001) layers that are 5 to 400 μm thick. These layers are surrounded by finer (101), (100), and minor (301) layers that are 1 to 5 μm thick. A small phantom crystal within the unlayered core displays prominent (100), (001), (101), and (301) crystal forms. The birefringence of individual layers varies as a function of uranium and thorium contents (*15*) as illustrated by variations in the interference colors (Fig. 2).

Department of Geology, University of New Mexico, Albuquerque, NM 87131.

*On leave from the Japan Atomic Energy Research Institute, Department of Environmental Safety Research, Tokai, Ibaraki 319-11, Japan.

The variation in birefringence (0.008 to 0.045) is due to alpha-decay damage (*3*) and can be used to estimate the alpha-decay dose (0.28×10^{16} to 0.70×10^{16} alpha-events per milligram), equivalent displacements per atom (0.21 to 0.53), and the density (4.56 to 4.16 g cm^{-3}) of individual layers (*15*). Electron microprobe analyses (*16*) across individual zones confirmed the systematic variation of UO_2 content (0.19 to 0.45% by weight) with birefringence (Fig. 2). The bulk property values of density and alpha-decay dose are in excellent agreement with the range of densities estimated from the birefringence measurements and the range of doses calculated from the electron microprobe analyses.

The zonation shows microfractures that are perpendicular to the zoning in bands of high birefringence (>0.02) and are absent in zones of low birefringence (≤ 0.02; equivalent to a UO_2 content of 0.3% by weight and a dose of 0.5×10^{16} alpha-events per milligram) (Fig. 2). The fracture

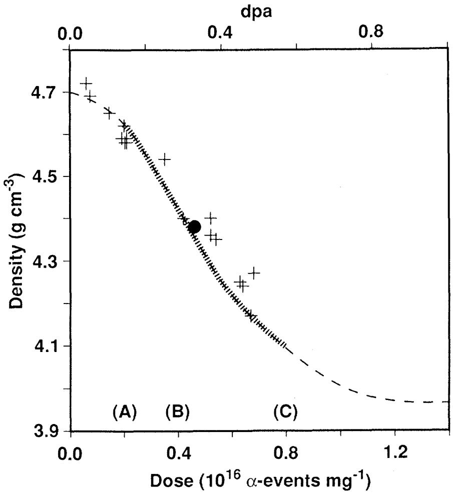

Fig. 1. Density as a function of alpha-decay dose and displacements per atom (dpa) for zircons from Sri Lanka. The dashed curve is a fit to the data from Holland and Gottfried (*3*). The crosses are data for other Sri Lankan zircons (*28*) and are displaced from the curve because the calculated dose also includes alpha-decay events in the ^{232}Th decay series [omitted by Holland and Gottfried (*3*)]. The bulk density of the sample, 4.38(1) g cm^{-3}, and the average alpha-decay dose, $0.46(2) \times 10^{16}$ alpha-events per milligram (α-events mg^{-1}), which were determined by instrumental neutron activation analysis on fragments of the crystal (*29*), are plotted as a solid circle. The hachured portion of the Holland and Gottfried curve is the range of dose for sample 4601 based on the UO_2 and ThO_2 contents that were determined by electron microprobe analysis. The range of dose as determined by the birefringence–uranium content relation of Sahama (*15*) is smaller (0.3×10^{16} to 0.7×10^{16} alpha-events per milligram). The letters at the bottom of the figure mark doses that correspond to the stages of damage ingrowth as shown by the high-resolution transmission electron micrographs in Fig. 3.

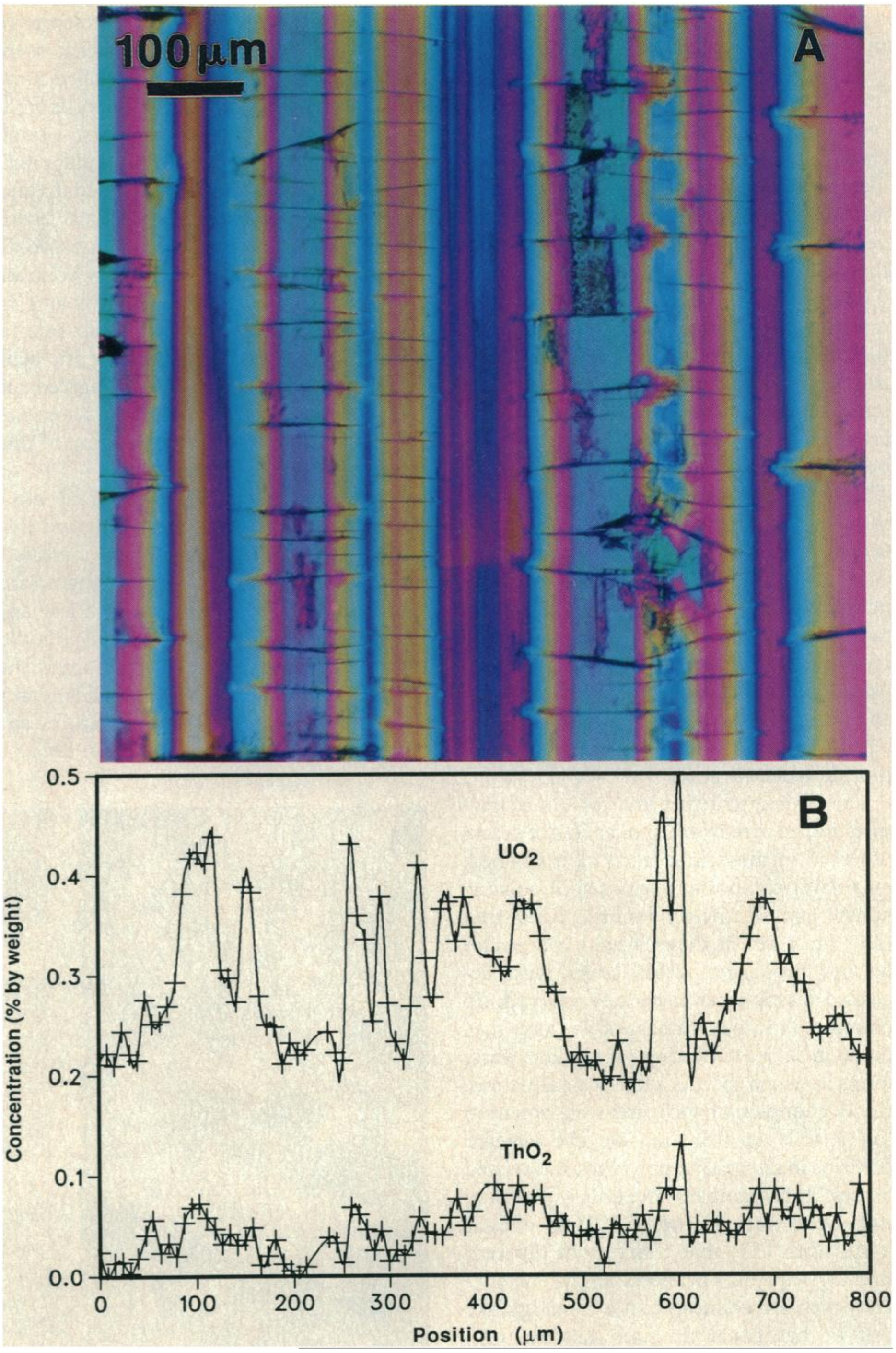

Fig. 2. (**A**) Optical micrograph of (001) zoning in a petrographic thin section (0.03 mm thick) of zircon sample 4601 viewed between crossed polarizing lenses. The field of view is 0.8 mm in diameter. The interference color (and hence birefringence) correlates with the UO_2 content as determined by Sahama (*15*). With increasing content of uranium and thorium, or of alpha-decay dose, the order of the interference colors (*30*), or birefringence, decreases and approaches a damage-saturated state when the birefringence is zero (isotropic). For this portion of the sample, the interference colors range from third-order green (birefringence of 0.040) to first-order yellow (birefringence of 0.012). The microfractures terminate in zones that display interference colors of second-order blue or lower, which corresponds to an alpha-decay dose of $\geq 0.5 \times 10^{16}$ alpha-events per milligram. (**B**) Concentrations of UO_2 and ThO_2 for a trace across (A) determined by electron microprobe analysis (EMPA). The ThO_2 content· is near the detection limit for the EMPA, but it varies (0.02 to 0.13% by weight) sympathetically with the UO_2 content. Moreover, the $UO_2 + ThO_2$ content correlates with the absence of fractures in the zones that have accumulated the most alpha-decay damage. Concentrations of Y_2O_3 (0.06 to 0.13% by weight) and P_2O_5 (0.06 to 0.12% by weight) are not shown, but their contents also vary sympathetically with the uranium content.

spacing is 42% (SE = 0.02) of the layer thickness in which the fractures occur. The fractures do not extend through the layers that received the highest alpha-decay dose ($\geq 0.5 \times 10^{16}$ alpha-events per milligram or ≥ 0.38 dpa). This is consistent with previous observations that the fracture toughness increases and elastic moduli decrease with increasing alpha-decay dose (*4, 17*). The microfracturing is the result of the stress generated by the anisotropic expansion of the unit cell (at saturation doses, $\Delta a/a = 0.01$ and $\Delta c/c = 0.025$) caused by the accumulation of interstitials that were created by the alpha-decay event (*3, 6, 18*). The anisotropic expansion may explain the near absence of fractures in the (100) and (101) layers. Similar microfracture patterns have been observed in zircon used in a recent U-Th-Pb dating study (*19*). These zircons show a concentric zoning of alternating layers of high and low uranium and thorium concentrations. Microfractures are prominent in the low alpha-decay dose layers and radiate from the core nearly perpendicular to crystal faces, presumably because of the expansion of the layers enriched in uranium and thorium. Some of the fractures are filled with a material with a high uranium and thorium concentration.

The layered structure and pattern of fractures in this zircon are similar to the cracks observed in the brittle layers of a strained, microlayer composite composed of polycarbonate and styrene-acrylonitrile copolymer (*20*). Fractures in these layered composites do not propagate across layers with decreased elastic moduli because of crack-tip blunting. A similar pattern of fractures may occur in actinide-bearing, crystalline waste forms in which there is a fine-scale zonation. Good examples of such fine-scale zonation (on a scale of 0.1 nm) are the lamellar domains in zirconolite polytypes and related phases (for example, zirconolite, zirkelite, and pyrochlore) in the SYNROC nuclear waste form (*12*) that result from different stacking sequences of sheets of TiO_6 octahedra which are connected in a topology like that of hexagonal tungsten bronze (*21*). Variations in actinide concentrations in individual lamellae may cause fracture patterns similar to those observed in this zircon because zirconolite is monoclinic and highly anisotropic in its volume expansion [up to 2.1% in curium-doped synthetic zirconolite (*22*)] with increasing alpha-decay dose (*13, 18*).

High-resolution transmission electron micrographs (HRTEM) of crushed grains (<1 μm in size) from the crystal revealed a range of damage microstructures (*23*). Figure 3 shows HRTEM and electron diffraction patterns of the (A) least, (B) intermediate, and (C) most damaged areas. Figure 1 shows their relative positions in terms of dose. These micrographs are representative of the three stages of damage that were distinguished on the basis of detailed x-ray diffraction analysis of a suite of zircons from Sri Lanka (*6*). In the first stage ($<0.3 \times 10^{16}$ alpha-events per milligram), the electron diffraction pattern is sharp and the HRTEM shows two-dimensional lattice fringes. The only evidence of alpha-decay damage is a "mottled" diffraction contrast (*8, 24*) and isolated aperiodic domains in which lattice fringes are almost absent. In rare instances lattice fringes are slightly bent or discontinuous. This is in good agreement with the value of 0.2×10^{16} alpha-events per milligram for the minimum dose of this sample. In the second stage (0.3×10^{16} to 0.8×10^{16} alpha-events per milligram) electron diffraction maxima are fainter and diffuse, which corresponds to the increased structural distortion. Lattice fringes are modulated and discontinuous with low angle boundaries between domains. Aperiodic areas (lattice fringes absent) are abundant but the distorted crystalline domains retain the same orientation. These structures are consistent with the measured mean dose of 0.46×10^{16} alpha-events per milligram. In the third stage ($>0.8 \times 10^{16}$ alpha-events per milligram) the electron diffraction pattern consists of diffuse rings and there is no evidence for long-range periodicity. In some fragments the powder diffraction rings that correspond to misoriented microcrystallites (1 to 10 nm) may be the result of alteration or recrystallization (*25*).

The HRTEMs show that in the earliest stages of the transition from the crystalline to metamict state the unit cell expands because interstitials are created [and are mainly associated with the alpha-particle damage that creates several hundred Frenkel defect pairs at the end of each track (*13*)] and the ingrowth of larger aperiodic regions [caused by the alpha-recoil nuclei which displace several thousand atoms per decay event (*13*)]. The conversion of the periodic array of atoms to an aperiodic array occurs when there is significant overlap of the alpha-recoil tracks ($>0.8 \times 10^{16}$ alpha-events per milligram or >0.6 dpa). The optimal dose at which an individual alpha-recoil track might be observed in a HRTEM would be at doses of $\sim 0.2 \times 10^{16}$ alpha-events per milligram, that is, prior to significant track overlap. In Fig. 3A, arrows point to areas in which

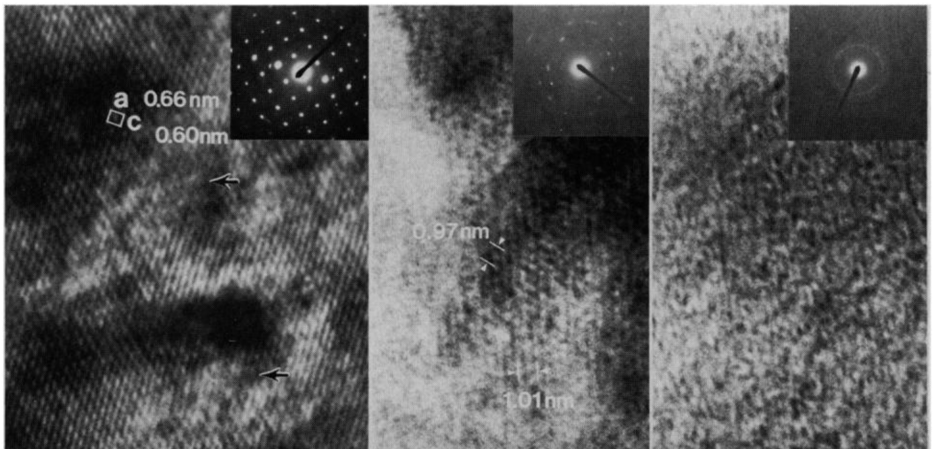

Fig. 3. High-resolution transmission electron micrographs and electron diffraction patterns of zircon sample 4601. (**A**) The least damaged area displays mottled diffraction contrast in the (101) plane. Two-dimensional lattice fringes are evident and a unit cell (a = 0.66 nm and c = 0.60 nm) is outlined. Some lattice fringes are bent and discontinuous. Examples of aperiodic domains (1 to 5 nm) in which lattice fringes are almost absent, possibly because of alpha-recoil tracks, are indicated by arrows. In spite of these bright-field features, the electron diffraction spots are sharp and clear. (**B**) The intermediately damaged area. The bright-field image is parallel to ($\bar{1}11$). The spots in the diffraction pattern are broad and diffuse, which corresponds to increased structural distortion. Although the aperiodic domains are as abundant as the domains of distinct lattice fringes, the distorted crystalline domains have the same orientation. Lattice dimensions are given for the [110] (1.01 nm) and [$0\bar{1}\bar{1}$] (0.97 nm) directions. (**C**) The most damaged area. The bright-field image shows no evidence for long-range periodicity. In addition to diffuse rings, the electron diffraction pattern has powder rings that result from misoriented microcrystallites. The arrow points to a microcrystallite displaying [100] (0.66 nm) lattice fringes.

lattice fringes are absent. If we assume that 2000 atoms are displaced by the alpha-recoil nucleus, we calculate that the maximum dimension of an alpha-recoil track is 2 to 5 nm. The measured size of the aperiodic areas in the HRTEMs is 1 to 5 nm. These aperiodic areas are similar in general appearance to the amorphous cascade regions in Bi^+-implanted silicon (*26*).

The radiation-induced structural change and resulting fractures caused by alpha-decay in this zircon may be the type that could occur in actinide-bearing, polyphase, ceramic nuclear waste forms. Additionally, this fine-scale variation in the alpha-decay dose may account in part for discordant ages from zircons determined by U-Th-Pb methods (*9*). The system of microfractures provides pathways for the addition or removal of uranium, thorium, and lead. In addition, damaged areas will be removed preferentially as a result of the increased solubility of metamict zircon compared to that of crystalline zircon (*27*).

REFERENCES AND NOTES

1. J. A. Speer, in *Orthosilicates*, P. H. Ribbe, Ed., *Reviews in Mineralogy* (Mineralogical Society of America, Washington, DC, ed. 2, 1982), vol. 5, pp. 67–105.
2. R. Tornhroos, *Bull. Geol. Soc. Finl.* **57**, 181 (1985).
3. H. D. Holland and D. Gottfried, *Acta Crystallogr.* **8**, 291 (1955).
4. H. Ozkan, *J. Appl. Phys.* **47**, 4772 (1976).
5. G. J. Exarhos, in *Radiation Effects in Insulators*, G. W. Arnold and J. A. Borders, Eds. (North-Holland, Amsterdam, 1984), pp. 538–541.
6. T. Murakami, B. C. Chakoumakos, R. C. Ewing, in *Advances in Ceramics, Nuclear Waste Management II*, D. E. Clark, W. B. White, J. Machiels, Eds. (American Ceramic Society, Columbus, OH, 1987), vol. 20, pp. 745–753.
7. L. A. Bursill and A. C. McLaren, *Phys. Status Solidi* **13**, 331 (1966); I. Y. Chan and P. R. Buseck, in *Proceedings of the 40th Meeting of the Electron Microscopy Society of America*, G. W. Bailey, Ed. (Claitor's, Baton Rouge, LA, 1982), pp. 618–619; T. J. Headley, R. C. Ewing, R. F. Haaker, in *Proceedings of 39th Meeting of the Electron Microscopy Society of America*, G. W. Bailey, Ed. (Claitor's, Baton Rouge, LA, 1981), pp. 112–113; T. Murakami, B. C. Chakoumakos, R. C. Ewing, in *14th Proceedings of the International Mineralogical Association* (Mineralogical Society of America, Washington, DC, 1986), p. 179; K. Yada, T. Tanji, I. Sunagawa, *Phys. Chem. Minerals* 7, 47 (1981); *ibid.* **14**, 197 (1987).
8. T. J. Headley, R. C. Ewing, R. F. Haaker, in *13th Proceedings of the International Mineralogical Association* (Bulgarian Academy of Science, Varna, Bulgaria, 1986), pp. 281–289.
9. T. E. Krogh, *Geochim. Cosmochim. Acta* **46**, 637 (1982); *ibid.*, p. 631; ______ and G. L. Davis, in *Carnegie Inst. Washington Yearb.* **74**, 619 (1975); ______, *ibid.* **73**, 560 (1974); R. T. Pidgeon, J. R. O'Neil, L. T. Silver, *Science* **154**, 1538 (1966); R. Steiger and G. J. Wasserburg, *J. Geophys. Res.* **71**, 6065 (1966).
10. A. B. Harker and J. F. Flintoff, in *Scientific Basis for Nuclear Waste Management VII*, G. McVay, Ed. (Elsevier, New York, 1984), vol. 26, pp. 513–520.
11. R. V. Gentry *et al.*, *Science* **216**, 296 (1982); K. R. Ludwig, R. E. Zartman, S. S. Goldich, *ibid.* **223**, 835 (1984); R. V. Gentry, *ibid.*, p. 835.
12. A. E. Ringwood, *Mineral. Mag.* **49**, 159 (1985); *Am. Sci.* **70**, 201 (1982).
13. G. R. Lumpkin *et al.*, *J. Mater. Res.* **1**, 564 (1986).
14. K. Dahanayake and A. P. Ranasinghe, *Bull. Geol. Soc. Finl.* **57**, 139 (1985); T. Munasinghe and C. B. Dissanayake, *Econ. Geol.* **76**, 1216 (1981); M. B. Katz, *ibid.* **67**, 113 (1972).
15. T. G. Sahama, *Bull. Soc. Fr. Mineral.* **104**, 89 (1981).
16. Polished sections of the zircon crystal were analyzed for as many as nine elements simultaneously by using a JEOL 733 Superprobe operated at 15 kV with a beam diameter of 2 μm. The detection limits and precision for minor elements were improved by using a sample current of 50 nA with counting times of up to 90 seconds for uranium and thorium. Minimum detection limits are approximately 100 ppm for aluminum, phosphorus, calcium, and yttrium; 150 ppm for thorium and uranium; and 200 ppm for cerium. Data were corrected for deadtime, drift, fluorescence, and absorption effects by using an empirical alpha-factor approach [A. E. Bence and A. L. Albee, *J. Geol.* **76**, 382 (1968); A. L. Albee and L. Ray, *Anal. Chem.* **42**, 1408 (1977)]. Standards included synthetic zircon (silicon, zirconium, and hafnium), synthetic thorite (thorium), YPO_4 (yttrium), $CePO_4$ (cerium and phosphorus), UO_2 (uranium), and anorthite (aluminum and calcium).
17. F. W. Clinard *et al.*, in *Scientific Basis for Nuclear Waste Management VIII*, C. M. Jantzen *et al.*, Eds. (Materials Research Society, Pittsburgh, 1985), vol. 44, pp. 663–670; R. C. Ewing, *Am. Mineral.* **58**, 942 (1973).
18. B. C. Chakoumakos and R. C. Ewing, *Geol. Soc. Am. Abstr. Programs* **17**, 542 (1985).
19. Z. E. Peterman, R. E. Zartman, P. K. Sims, *U.S. Geol. Surv. Bull.* **1622**, 51 (1986).
20. E. Baer, A. Hiltner, H. D. Keith, *Science* **235**, 1015 (1987).
21. T. J. White, *Am. Mineral.* **69**, 1156 (1984); ______, R. L. Segall, J. L. Hutchinson, J. C. Barry, *Proc. R. Soc. London Ser. A* **392**, 343 (1984).
22. J. W. Wald and P. Offerman, in *Scientific Basis for Nuclear Waste Management V*, W. Lutze, Ed. (North-Holland, New York, 1982), vol. 11, pp. 369–378.
23. Powdered aliquots of the zircon crystal were dispersed in methanol and sampled with holey carbon-filmed, copper grids. Specimens were examined by using a JEOL 2000 FX transmission electron microscope operated at 200 kV.
24. G. R. Lumpkin and R. C. Ewing, in *Microbeam Analysis 1986*, A. D. Romig, Jr., and W. F. Chambers, Eds. (San Francisco Press, San Francisco, 1986), pp. 145–146.
25. T. J. Headley and R. C. Ewing, *ibid.*, pp. 141–144.
26. J. Narayan *et al.*, *Mater. Lett.* **3**, 67 (1985).
27. R. C. Ewing *et al.*, in *Scientific Basis for Nuclear Waste Management V*, W. Lutze, Ed. (North-Holland, New York, 1982), vol. 11, pp. 389–396; M. P. Tole, *Geochim. Cosmochim. Acta* **49**, 453 (1984).
28. T. Murakami, B. C. Chakoumakos, G. R. Lumpkin, R. C. Ewing, unpublished results.
29. Uranium and thorium contents were determined by instrumental neutron activation analysis on a 28.9-mg fragment of the sample. A delayed neutron counting technique, which counts delayed neutrons from the fission of ^{235}U, was used for the total uranium assay by assuming a natural abundance of 0.72% for ^{235}U. The analysis was completed at Los Alamos National Laboratory by S. R. Garcia.
30. Interference colors are divided into orders according to whether they result from retardations of 0 to 550 μm (first-order colors), 550 to 1100 μm (second-order colors), 1100 to 1650 μm (third-order colors), and so on.

31. Electron microprobe analyses and the transmission electron microscopy were completed in the Electron Microbeam Analysis Facility in the Department of Geology and Institute of Meteoritics at the University of New Mexico, supported in part by the NSF, NASA, DOE–Basic Energy Sciences, and the state of New Mexico. This work was supported by the U.S. Department of Energy, Office of Basic Energy Sciences (grant DE-FG04-84ER45099) and Sandia National Laboratories. The instrumental neutron activation analyses were completed at Los Alamos National Laboratory by the Research Reactor Group by S. R. Garcia (Los Alamos National Laboratories) and H. E. Newsom (University of New Mexico).

24 March 1987; accepted 7 May 1987

Acid Rain: China, United States, and a Remote Area

JAMES N. GALLOWAY, ZHAO DIANWU, XIONG JILING, GENE E. LIKENS

The composition of precipitation in China is highly influenced by fossil fuel combustion and agricultural and cultural practices. Compared to the eastern United States, precipitation in China generally has higher concentrations of sulfate, ammonium, and calcium. Wet deposition rates of sulfur in China are 7 to 130 times higher than those in a remote area in the Southern Hemisphere. In many areas of the world, significant ecological changes have occurred in ecosystems that have acid deposition rates substantially less than those currently existing in China.

THE IMPACT OF ANTHROPOGENIC activities on precipitation composition and the subsequent effects on aquatic and terrestrial ecosystems have been investigated in North America, Scandinavia, and Europe over the past decade (*1*). However, only recently have data been available on the composition of precipitation in China (*2–5*). These data indicate that the composition of this precipitation is also strongly influenced by anthropogenic activities. To evaluate the degree of influence and the potential ecological effects on aquatic and terrestrial ecosystems, we compared the precipitation composition in China, the eastern United States, and a remote area in the Southern Hemisphere (Katherine, Australia). The ecological implications of these observed differences in precipitation composition are presented here.

J. N. Galloway, Department of Environmental Sciences, University of Virginia, Charlottesville, VA 22903.
Zhao Dianwu, Institute of Environmental Chemistry, Academia Sinica, P.O. Box 934, Beijing, China.
Xiong Jiling, Guizhou Institute of Environmental Sciences, Xinghua Road, Guiyang, China.
G. E. Likens, Institute of Ecosystem Studies, New York Botanical Garden, Millbrook, NY 12545.